

# Quantitative Evaluation of Scatter Correction in 128-slice Fan-Beam Computed Tomography Scan using Geant4 Application for Tomographic Emission Monte Carlo Simulation

## Abstract

**Background:** Simulation of tomographic imaging systems with fan-beam geometry, estimation of scattered beam profile using Monte Carlo techniques, and scatter correction using estimated data have always been new challenges in the field of medical imaging. The most important aspect is to ensure the results of the simulation and the accuracy of the scatter correction. This study aims to simulate 128-slice computed tomography (CT) scan using the Geant4 Application for Tomographic Emission (GATE) program, to assess the validity of this simulation and estimate the scatter profile. Finally, a quantitative comparison of the results is made from scatter correction. **Methods:** In this study, 128-slice CT scan devices with fan-beam geometry along with two phantoms were simulated by GATE program. Two validation methods were performed to validate the simulation results. The data obtained from scatter estimation of the simulation was used in a projection-based scatter correction technique, and the post-correction results were analyzed using four quantities, such as: pixel intensity, CT number inaccuracy, contrast-to-noise ratio (CNR), and signal-to-noise ratio (SNR). **Results:** Both validation methods have confirmed the appropriate accuracy of the simulation. In the quantitative analysis of the results before and after the scatter correction, it should be said that the pixel intensity patterns were close to each other, and the accuracy of the CT scan number reached <10%. Moreover, CNR and SNR have increased by more than 30%–65% respectively in all studied areas. **Conclusion:** The comparison of the results before and after scatter correction shows an improvement in CNR and SNR while a reduction in cupping artifact according to pixel intensity pattern and enhanced CT number accuracy.

**Keywords:** Correction, computed tomography, geant4 application for tomographic emission, scatter

Submitted: 23-Dec-2022

Revised: 19-Mar-2023

Accepted: 09-May-2023

Published: 31-Aug-2023

## Introduction

Computed tomography (CT) scan imaging equipment has always been one of the most important medical modalities in the diagnostic field.<sup>[1]</sup> Therefore, researchers have always been trying to increase the efficiency of this equipment regarding image quality and especially in the field of reducing artifacts. Scatter radiation, which has always been a big challenge, is one of the important topics in the field of image quality in CT scan. The challenge of scatter rays in single-slice CT scan device was very evident, although this generation of CT scan did not have a high radiation volume, due to the weakness of the equipment to rejection scatter rays, its effects were very clear. Many studies have been done in the field

of scatter rays<sup>[2,3]</sup> and it should be said in general, they mainly lead to shading artifacts and CT number inaccuracy in reconstructed images.<sup>[4-7]</sup> Shading artifacts mainly include two categories: In the first category, the reduction of attenuation coefficients in a reconstructed CT scan image leads to nonuniformity and causes a cup shape in the image, which is known as a cupping artifact.<sup>[8]</sup> In the second category, the same situation happens between two very dense objects and forms dark bands. In this case, the bands are called streak artifacts.<sup>[9,10]</sup> Scatter rays challenge in cone-beam CT scans is more severe than it is in fan-beam CT scans due to their geometric nature and more radiation volume. However, in multi-slice CT scans, the increase in the number of detectors and irradiation volume have resulted in an increase in the scatter

Iman Azinkhah<sup>1</sup>,  
Mahdi Sadeghi<sup>1</sup>,  
Peyman  
Sheikhzadeh<sup>2</sup>,  
Malakeh  
Malekzadeh<sup>3</sup>

<sup>1</sup>Finetech in Medicine Research Center, Department of Medical Physics, School of Medicine, Iran University of Medical Sciences, <sup>2</sup>Department of Nuclear Medicine, Imam Khomeini Hospital Complex, Tehran University of Medical Sciences, <sup>3</sup>Department of Medical Physics, School of Medicine, Iran University of Medical Sciences, Tehran, Iran

**Address for correspondence:**  
Prof. Mahdi Sadeghi,  
Department of Medical Physics,  
School of Medicine, Iran  
University of Medical Sciences,  
P. O. Box: 14155-6183, Tehran,  
Iran.  
E-mail: sadeghi.m@iums.ac.ir

Access this article online

Website: www.jmssjournal.net

DOI: 10.4103/jmss.jmss\_71\_22

Quick Response Code:



**How to cite this article:** Azinkhah I, Sadeghi M, Sheikhzadeh P, Malekzadeh M. Quantitative evaluation of scatter correction in 128-slice fan-beam computed tomography scan using geant4 application for tomographic emission Monte Carlo simulation. J Med Sign Sens 2023;13:280-9.

This is an open access journal, and articles are distributed under the terms of the Creative Commons Attribution-NonCommercial-ShareAlike 4.0 License, which allows others to remix, tweak, and build upon the work non-commercially, as long as appropriate credit is given and the new creations are licensed under the identical terms.

For reprints contact: WKHLRPMedknow\_reprints@wolterskluwer.com

fraction.<sup>[11]</sup> Furthermore, the use of flat detectors can increase the scatter fraction up to 100%.<sup>[5]</sup> For this reason, various approaches, which can generally be considered in two groups, have been introduced to reduce the effect of scatter rays: scatter rejection and scatter correction.<sup>[12]</sup> Rejection techniques are mainly hardware techniques for rejection scatter rays, these hardware techniques include some physical equipment such as a collimator, bow-tie filter, air gap, and anti-scatter grid. However, this equipment is not enough to completely rejection scatter rays. As in a comprehensive study of the effect of scatter rays on CT images conducted by Siewerdsen and Jaffray,<sup>[5]</sup> the importance of using software methods to rejection scatter has been emphasized even after using physical equipment. However, correction techniques include two categories: Scatter estimation and scatter compensation.<sup>[13]</sup> In the scatter compensation techniques, the main goal is to improve the image quality by using multiple reconstructions to reduce the effect of scatter in images. However, scatter estimation techniques are mainly based on mathematical models to estimate scatter and finally remove this information from the final images. One of the most interesting approaches in scatter estimation is to use Monte Carlo techniques. Due to the random nature of X-ray-matter interactions and scatter process, Monte Carlo techniques have become very useful and many estimations and simulations have been powered by them.<sup>[14-18]</sup> Recently, Monte Carlo has become one of the most common techniques in X-ray simulation studies; especially in scattered radiation estimation.<sup>[19]</sup> GEANT4 (Geometry and Tracking) is one of the Monte Carlo-based programs,<sup>[20]</sup> which has been superiorly successful in simulating medical imaging and treatment equipment. A more specialized software package based on this program, called Geant4 Application for Tomographic Emission (GATE), was provided for simulating tomographic imaging equipment.<sup>[21]</sup> The main purpose of this study is to use Monte Carlo GATE techniques to check the effectiveness of these methods in scatter correction from CT scan images. This study consists of four parts, the first part is to simulate a 128-slice multi-CT scan with fan-beam geometry using the GATE program, also, the simulation of a quality control phantom of the device itself so that we can compare the experimental results with the simulation results in a more appropriate way. In the second part, we need methods to measure the validity of GATE simulation with a CT scan device, which was examined in this study with two approaches. One is the method of lead blocks and the other is the method of checking the intensity profile of pixels in the phantom. In the third part, after confirming the validation results, the information related to the estimated scatter rays was extracted and a scatter correction method was applied on the CT images taken. And finally, in the final part, the qualitative and quantitative results of this scatter correction were studied by comparing the quality control phantom images before and after the scatter correction.

## Materials and Methods

### Computed tomography scan

The chosen device for simulating is PHILIPS Ingenuity Core 128 with fan-beam geometry. The specifications of the device are as follows: focus to isocenter distance is 570 mm and focus to detector distance is 1040 mm. The maximum kVp is 140, the anode angle is 7°, and it has a 2.5 mm aluminum filter. The focal point is equal to 0.5 mm × 1.0 mm and 1.0 mm × 1.0 mm, according to the IEC 93/336 standard. The detector, which is also an important part of the simulation, is made of Solid-State Gadolinium Oxysulfide ( $Gd_2O_2S$ ) with 43008 elements and the smallest thickness of 0.625 mm. According to the number of detector rows (64) and the thickness of each detector element (0.625 mm), the maximum Field of View (FOV) of the device is 500 mm. To define the fan-beam geometry system, a separate macro file called collimator was written so that we could implement fan-beam geometry in the simulation. The defined collimator includes a trapezoidal geometry made of lead with a trapezoidal opening in the middle for X-ray output. The opening was calculated and programmed to match completely with the detectors area according to critical distances of the source to detector and isocenter. SPEKTR 3.0<sup>[22]</sup> program was implemented for X-ray spectrum calculation. Considering that the CT device has 80,100,120, and 140 kVp, the spectrum was calculated for each of four kVp with Al filter and included in the X-ray source macro file of GATE program. Figure 1 illustrates the general geometry of this program.

### Phantoms

Two phantoms were used in this study. The quality control head phantom of the device was also utilized to control the results of the simulation and to compare the experimental results of the CT scan device with the simulation done with GATE. The head phantom consists of three layers: physical layer, water layer, and multi-pin layer. The multi-pin layer has pins made of different materials, some of which were not available in the material database of the GATE program. Hence, the information on these materials was added to the material database includes: Teflon, Nylon, Polyethylene, Lexan, and Acrylic. Furthermore, a simple cylindrical phantom with a diameter of 300 mm and a height of 200 mm was simulated exactly the same as the

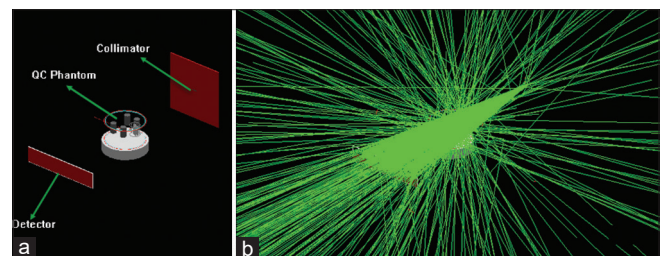


Figure 1: Geometry of collimator, phantom and detector in GATE (a), The same geometry in the simulation environment (b). GATE – Geant4 Application for Tomographic Emission

water phantom of the device. Figure 2a and b illustrate the real phantom of the CT scan and Figure 2c and d show the simulation phantom image in the OpenGL environment.

### Geant4 application for tomographic emission

For simulation, GATE program<sup>[23]</sup> version 9.1, which is compatible with GEANT4 version 9 program (CERN, Geant4 Collaboration, Meyrin, Switzerland), was used. The simulation hardware system included a Core i5 central processing unit with 8GB of RAM. The macro writing capability of the GATE program was used for the simulation process, and a main macro called and executed all the other structural macros, including visualization, world, phantom, scanner, collimator, physics list, digitizer, and source macros. Since the main goal of this simulation is to obtain scatter information, all possible scatterings in the diagnostic physics range were selected in the physics macro file. This includes PenelopeModel<sup>[24]</sup> cases for Compton, Rayleigh, and multiple scattering models. All simulations were done with 360 projections.

### Analysis and output data

In this study, we need both quantitative and visual qualitative information. Therefore, two outputs were set in the macro file of the GATE program. The first output of the ROOT<sup>[25]</sup> file is for accessing quantitative simulation information, and the second output is the DAT file for reconstructing the simulation projections to create a final CT image. Dat files, containing binary information in each projection, were reconstructed using the OMEAG<sup>[26]</sup> program, and the axial images were saved in DICOM format. Image reconstruction was done using MATLAB-based OMEGA program with the following conditions: Back Projection, FOV 400 mm,

isocenter to detector distance 560 mm, X-ray source to detector distance 1040 mm. Then, all computational measurements were performed by ImageJ<sup>[27]</sup> program using reconstructed images from GATE simulation.

### Simulation validation

We took two approaches to check the reliability and accuracy of the simulation done by GATE. In the first method, a water phantom and lead blocks with different diameters were used to measure scatter-primary ratio (SPR). Lead blocks with diameters of 10–50 mm were placed on the water phantom, and a one-projection scan was done on the water phantom with and without lead blocks. Then, radiation intensity was measured in the shadow of the lead blocks, being equivalent to the scatter rays. The radiation intensity was then measured in the same area without the lead blocks, which indicates the intensity of scatter and primary rays. Finally, by subtracting scatter and primary radiation intensity from scatter radiation intensity, the intensity of the primary rays will be obtained. Accordingly, we calculated the SPR for each diameter of the lead blocks, then the SPR for other diameters was interpolated. Then we calculated a fitting linear coefficient for it. All these steps were simulated under the same condition in the GATE program by acquiring one projection of a phantom with and without a lead block. Thus, the linear coefficients of the simulation condition SPRs were measured and compared with that of experimental examinations. The second method is to use a quality control phantom and to compare the intensity pattern of the simulated image with the image obtained from the experiment performed with CT scan. To compare the images, we obtained the intensity pattern of a row of pixels in both real and simulated phantom images and then compared them to each other. A row at the top related to Lexan and polyethylene densities, and a row at the bottom related to the acrylic and Teflon densities were measured.

### Scatter correction

To perform scatter correction, a projection-based correction method along with a Monte Carlo-based scatter estimation was used. The subtractive technique was used for scatter compensation stage. This estimation was done by simulating the CT scan device and its quality control phantom. However, one of the characteristics of scatter rays, which are considered a positive point in this section, is that the distribution of scatter X-rays is predominantly in low frequencies. Given this fact, small differences in an object should not have an effect on the scatter signal. Therefore, we can use primary radiation signal more confidently to correct the scattering.<sup>[28]</sup> For scatter correction, in this study, the CT scan scatter signal intensity is estimated from that of simulated scattering. For this, CT scan simulation was performed for the head part of the phantom, and the information related to the scatter rays  $I_{sim}^{scatter}(i,j)$  and the primary rays  $I_{sim}^{primary}(i,j)$  of each pixel were separated from each other according to  $(i,j)$  axes. Due to the high noise and weaker signal of scatter rays, we applied a smoothing filter to make the information smoother.

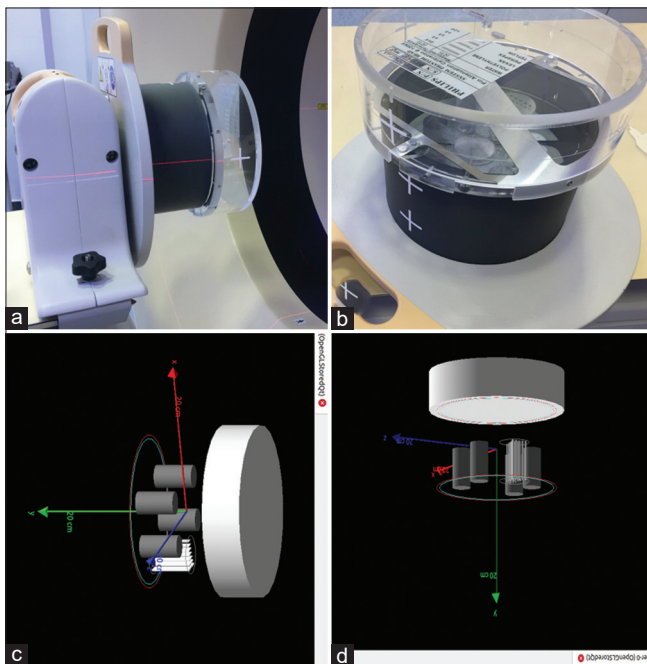


Figure 2: Real phantom in computed tomography (a and b), the same phantom in the simulation environment (c and d)



$$I_{sim}^{scatter}(i,j) \times \text{filter}_{low-pass}^{Gaussian} = I_{sim}^{scatter'}(i,j) \quad (1)$$

Then, by the following formula (2), the real or experimental scatter  $I_{real}^{scatter}(i,j)$  was estimated using the simulated scatter using filtered GATE  $I_{sim}^{scatter'}(i,j)$ :

$$I_{real}^{scatter}(i,j) = I_{sim}^{scatter'}(i,j) \times \left( \frac{I_{0(real)}(i,j)}{I_{0(sim)}(i,j)} \right) \quad (2)$$

Here,  $(i,j)$  is the coordinates of the pixel in the CT scan detector,  $I_{sim}^{scatter'}(i,j)$  is the simulated scatter signal intensity with the filter applied to reduce noise,  $I_{0(real)}(i,j)$  and  $I_{0(sim)}(i,j)$  are X-ray signal intensities from real CT scan and simulation, respectively, without phantom. Eventually, the corrected signal intensity can be calculated by subtracting the estimated scatter signal obtained from the simulation with phantom, i.e.,  $I_{real}^{scatter}(i,j)$  from the signal intensity measured in the CT scan exam with the phantom, i.e.,  $I_{real}(i,j)$ .<sup>[29]</sup>

$$I_c(i,j) = I_{real}(i,j) - I_{real}^{scatter}(i,j) \quad (3)$$

Thus, we obtain the corrected signal intensity of each pixel according to the Eq. 3 and reconstruct the final corrected image.

### Evaluation of scatter correction in reconstructed computed tomography scan images

Contrary to conventional procedures in these studies, in which the scatter correction is evaluated at single-projection images level, in this study, we assessed the effect of scatter correction on the final reconstructed image.

#### Evaluation of pixel intensity

In the first approach, the effect of scatter correction was investigated on pixel intensity in the phantom. Figure 3a-f

show axial images of the phantom before and after scatter correction, respectively. In order to compare the intensity of the pixels, three areas were examined linearly. The first row corresponds to the upper line of the phantom, passing through Lexan and polyethylene densities. The middle row passes through water, while the bottom row goes through Teflon and acrylic densities. Then, pixels intensities were measured in these rows on the phantom image in two modes: with scatter and scatter correction, then plotted on a graph for better comparison.

#### Evaluation of the computed tomography number inaccuracy

We investigated the impact of scatter correction on the CT numbers (Hounsfield) of different areas of the phantom. For this purpose, the CT numbers of five areas in the phantom including water, Lexan, acrylic, Teflon, and polyethylene were investigated [Figure 4]. The standard CT numbers of these five areas were extracted from the available information in the phantom and device booklets. Therefore, we considered them as reference CT numbers to compare between the device and performed simulation.

#### Evaluation of contrast-to-noise ratio

In order to investigate the effect of scatter correction on contrast-to-noise ratio (CNR) of CT scan images, the following formula was used:

$$CNR = \frac{|ROI_{obj} - ROI_b|}{\sqrt{(SD_{obj})^2 + (SD_b)^2}} \quad (4)$$

$ROI_{obj}$  is the CT number in the phantom absorption pin,  $ROI_b$  is the CT number outside the pin, i.e., the background of the phantom,  $SD_b$  is the standard deviation outside the pin, and  $SD_{obj}$  is the standard deviation of the pin itself.

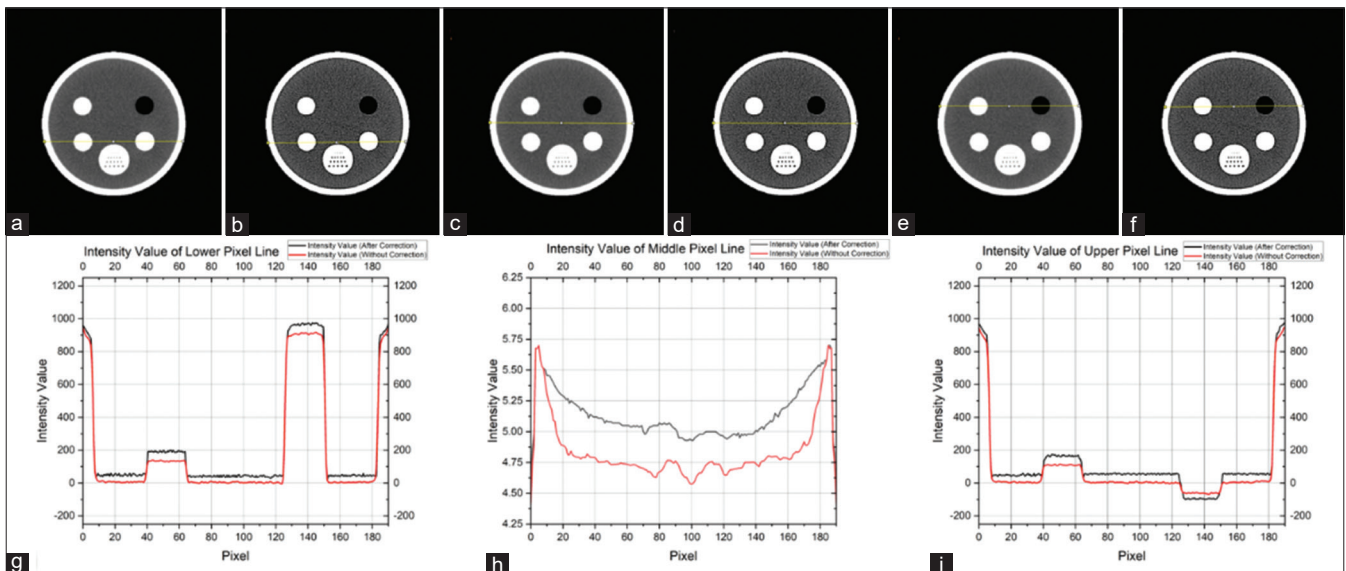


Figure 3: Pixel intensity evaluation before (a, c and e) and after (b, d and f) scatter correction in CT images. The graphs correspond to the intensity of the pixels in the bottom (g), middle (h) and top (i) line of the phantom before scatter correction (red) and after scatter correction (black)

*Evaluation of signal-to-noise ratio*

To evaluate this quantity, the water layer of the phantom was examined using the following formula:

$$SNR = \frac{\text{Mean Signal ROI}}{\text{SD ROI}} \quad (5)$$

Pixel intensity values and standard deviations were measured in 5 region of interest (ROI) including: The top, bottom, left, and right parts near the edge as well as the area in the center of the water phantom. Signal-to-noise ratio (SNR) calculations in the same previously mentioned five areas of the image are

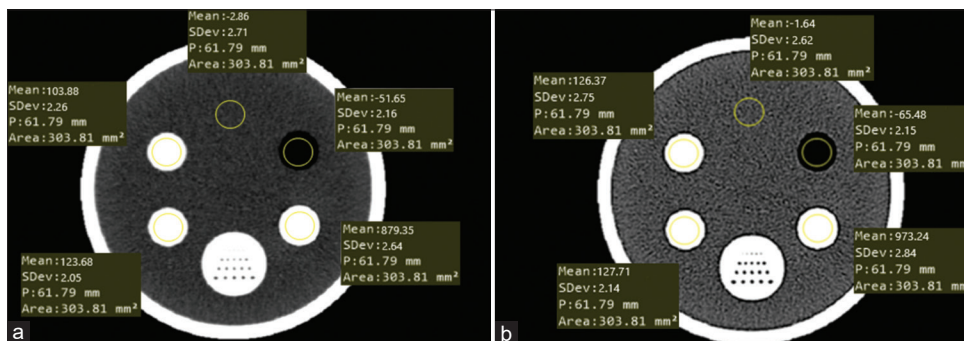


Figure 4: CT number values in five ROIs of Lexan, acrylic, Teflon, polyethylene and water in the images before (a) and after (b) scatter correction. ROI – Regions of interest; CT – Computed tomography

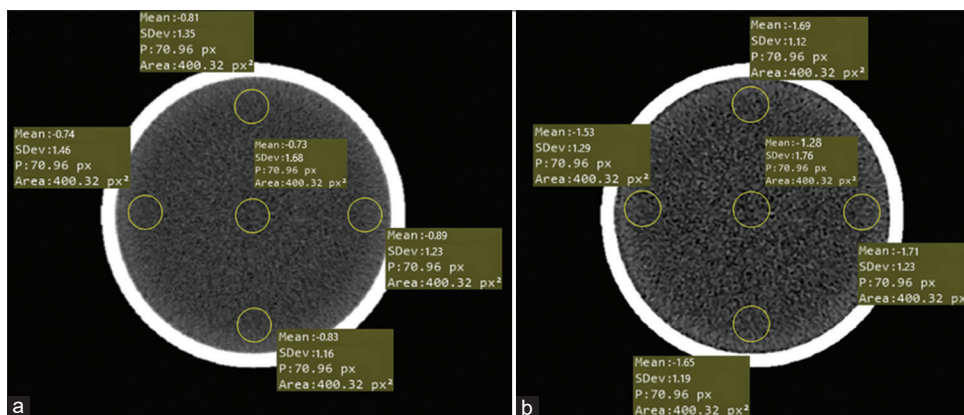


Figure 5: Pixel intensity values and standard deviations were measured in 5 ROIs in water phantom for calculation of SNR before (a) and after (b) scatter correction. ROI – Regions of interest; SNR – Signal-to-noise ratio

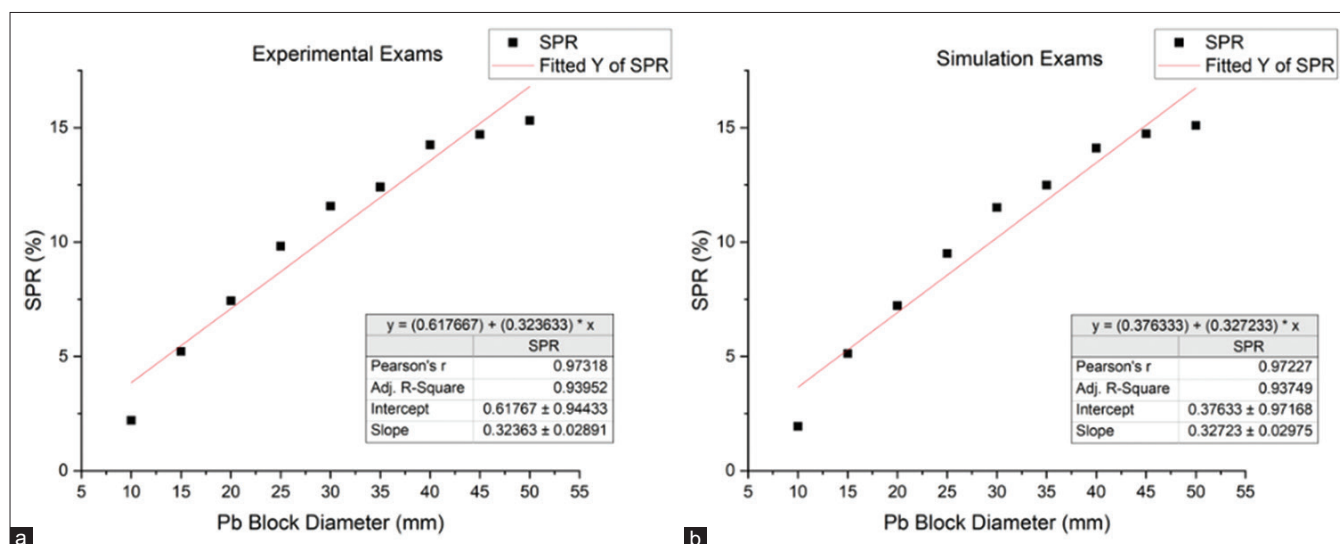


Figure 6: SPR graph and linear coefficient of both experimental (a) and simulation (b) exams. SPR – Scatter-primary ratio

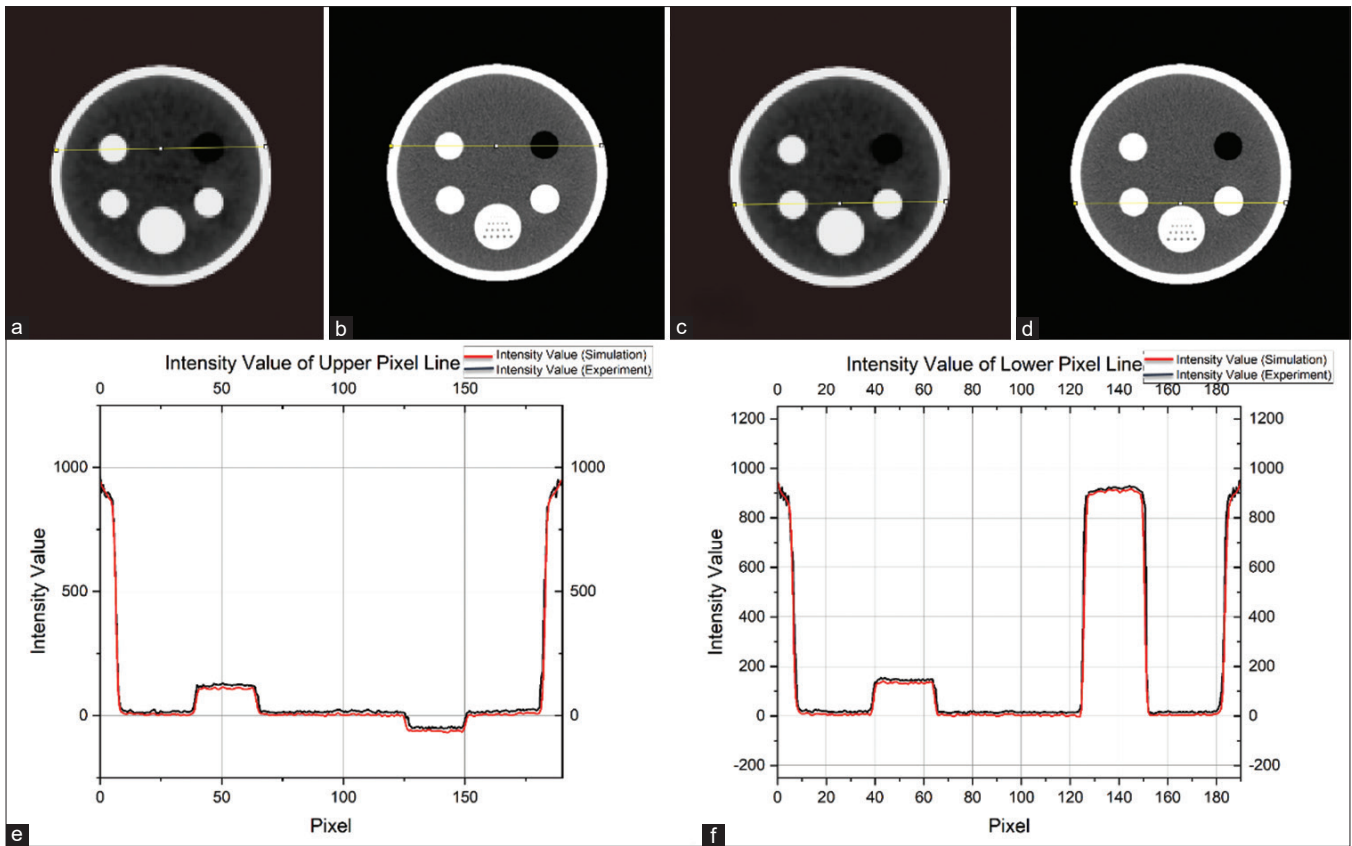


Figure 7: The intensity profile of the upper (e) and lower (f) pixels row in the simulation (a, c) and real (b, d) CT image. CT – Computed tomography

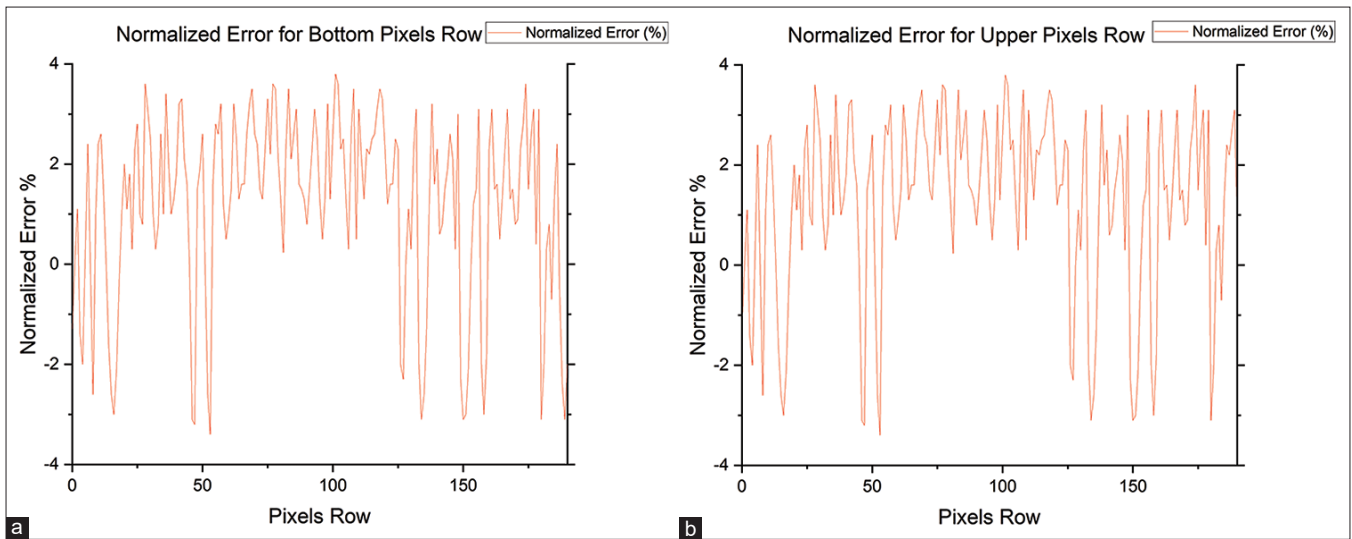


Figure 8: Calculated normalized error between simulation and real measurement in the bottom (a) and upper (b) Pixel row of the CT scan phantom. CT – Computed tomography

demonstrated in Figure 5a and b before and after scatter correction, respectively.

## Results

### Results of validation using lead block method

Figure 6 illustrates the SPR graph and linear coefficient of both simulation and experimental methods. The linear

coefficient in block simulation and experimental exam is equal to 0.97227 and 0.97318, respectively. There is no significant difference between them statistically.

### Results of validation using simulated phantom method

Figure 7f shows the intensity profile of bottom row pixels that relates to Acrylic and Teflon pins in the simulation [Figure 7c] and real [Figure 7d] image. The

black and red graph corresponds to intensity values in the experiment and simulated axial CT images, respectively. It is evident that these two graphs follow a similar pattern. In Figure 7a and b, the top rows are related to Lexan and polyethylene pins of the axial images obtained from the simulation and real scans, respectively. Figure 7e illustrates the intensity profile of the top row pixels of the phantom. In addition, it is obvious that these two graphs, similar to graphs for bottom rows of the phantom, share the same pattern. To better understand the validity of the simulation with real measurements, in addition to the comparison of the reduction profile of the simulation with the experimental reduction profile, a comparison based on the normalized error (NE) was also performed. In this way, the relative difference between the simulation data and the real measured data is calculated. This calculation was done according to Eq. 6 and usually, the difference between simulation and real measurement should be <4%.<sup>[30]</sup>

$$NE : \frac{PI_{real}(x,y) - PI_{simulation}(x,y)}{PI_{real}(x,y)} \quad (6)$$

In this equation,  $PI_{simulation}(x,y)$  and  $PI_{real}(x,y)$  are the pixel intensity in simulation and real measurement, respectively. Figure 8 shows the normalized error between real measurement and GATE simulation. The normalized error has been calculated both for the intensity profile of the pixels in the lower [Figure 8a] and upper [Figure 8b] row of the phantom.

### Results of pixel intensity evaluation after scatter correction

The first method of evaluating scatter correction using estimation-based Monte Carlo by GATE is to assess

pixel intensity in axial images before and after the scatter correction. We considered three rows on CT scan quality control phantom for comparison. The bottom row passes through Acrylic and Teflon materials [Figure 3a and b], the middle row only contains water [Figure 3c and d], and the top row [Figure 3e and f] passes through Lexan and Polyethylene (PE) materials. The first peak in the bottom row in the graph [Figure 3g] within the range of pixels 40–70 is related to the acrylic, and the second peak in the range of pixels 125–155 corresponds to the Teflon area. Given the high number of Hounsfield unit for Teflon, the second peak is the highest peak. In the remaining sections of the phantom, a more uniform trend close to the Hounsfield number of water is expectedly seen due to the fact that the phantom volume is filled with water. Considering that the middle line only passes through the water area, no specific peak can be seen in its diagram [Figure 3h]. However, the effect of scatter correction (black diagram) can be readily understood by paying attention to pixel intensity before the correction (red diagram). The first peak in the upper row [Figure 3i] within the range of pixels 40–70 is related to the Lexan material. The second peak, which is reversed, in the range of pixels 125–155 is related to polyethylene. Due to the low Hounsfield number of PVC, the inversion of this area was expected.

### Results of computed tomography number inaccuracy evaluation after scatter correction

In this section, the reference CT numbers were considered to be those values measured and mentioned on the phantom body by the supplier company. CT number values were measured in five ROIs of Lexan, acrylic, Teflon, polyethylene, and water in the images before and after scatter correction shown respectively in Figure 4a and b.

**Table 1: Computed tomography number values in five regions of interest in the images before and after scattering correction**

Phantom material	Standard CT number	Reference CT number	CT number measured from reconstructed images			
			Before scatter correction	Difference with reference CT number (%)	After scatter correction	Difference with reference CT number (%)
Lexan	120±15	116±5	103.88	10.44	126.37	8.93
Acrylic	130±15	135±5	123.68	8.38	127.71	5.40
Teflon	1045±45	992±5	879.35	11.35	973.24	1.89
Polyethylene	-60±15	-61±5	-51.65	15.32	-65.48	7.34
Water	0±4	-1.6±5	-2.86	78.75	-1.64	2.5

CT – Computed tomography

**Table 2: Calculated contrast-to-noise ratio for all four phantom absorption pins before and after scatter correction**

Phantom material	CT number measured from reconstructed images		SD measured from reconstructed images		CNR before scatter correction	CNR after scatter correction	CNR difference percentage before and after scatter correction (%)
	Before scatter correction	After scatter correction	Before scatter correction	After scatter correction			
Lexan	104.23	126.74	3.28	2.68	23.25	35.11	51.01
Acrylic	123.16	127.69	8.26	6.37	14.04	18.20	29.62
Teflon	880.35	973.58	32.62	26.52	26.89	36.61	36.14
Polyethylene	-51.89	-65.59	3.16	1.98	11.49	20.08	74.76

SD – Standard deviation; CNR – Contrast-to-noise ratio; CT – Computed tomography



**Table 3: Calculated signal-to-noise ratio along with the percentage of signal-to-noise ratio difference between before and after scatter correction**

ROI area in the water phantom	Before scatter correction			After scatter correction			SNR difference percentage before and after scatter correction (%)
	Mean signal ROI	SD	SNR	Mean signal ROI	SD	SNR	
Upper ROI	-0.81	1.35	0.60	-1.69	1.12	1.50	150.05
Bottom ROI	-0.83	1.16	0.71	-1.65	1.19	1.38	94.36
Right ROI	-0.74	1.46	0.51	-1.53	1.29	1.18	131.37
Left ROI	-0.89	1.23	0.72	-1.71	1.23	1.39	93.05
Middle ROI	-0.73	1.68	0.43	-1.28	1.76	0.72	67.44

SD – Standard deviation; ROI – Regions of interest; SNR – Signal-to-noise ratio

It is clear from Table 1 that in all five areas in images the percentage of difference in measured CT numbers has decreased after scatter correction and they have got closer to their reference values. This difference reduction has been much greater for the Teflon and water regions, which are equal to 1.89% and 2.50%, respectively.

### Results of contrast-to-noise ratio evaluation after scatter correction

Table 2 shows the calculated CNR for all four phantom absorption pins, namely Lexan, Acrylic, Teflon, and PVC. The highest values of CNR before and after scatter correction are both related to Teflon pin with a CNR of 26.89 and 36.61, respectively. The highest increase in CNR is related to polyethylene contrast after scatter correction. CNR increase can be seen in all absorption pins after scatter correction with a value of 51.01%, 29.62%, 36.14%, and 74.76%, for Lexan, acrylic, Teflon, and PVC, respectively.

### Results of signal-to-noise ratio evaluation after scatter correction

Calculated SNRs along with the percentage of SNR difference between before and after scatter correction are presented in Table 3 to better compare the correction process result. Calculated SNRs based on five ROIs and Eq. 5 by attention to Figure 5. The highest SNRs before scatter correction are related to the left (0.72) and bottom (0.71) ROIs, while after the process they belong to the left (1.39) and top (1.5) of the phantom. SNR improvement is obvious in all areas. However, the highest and the lowest increases in SNR are related to the top and the center ROIs with 150.05%–67.44% of improvement, respectively.

## Discussion

The use of GATE program and Monte Carlo techniques for simulating tomographic imaging systems is expanding day by day. However, it seems there is less research in simulating modern fan-beam geometry CT scans. Furthermore, one of the potential challenges of Monte Carlo techniques is the prolonged simulation times due to its nature, making it practically lose application in the clinical environment.<sup>[10]</sup> Nevertheless, with the advancement of the computing power of hardware, we can say that

performing Monte Carlo-based simulations with application in medicine is not a big obstacle today.<sup>[11,31-35]</sup> One of the most important aspects of a successful simulation is the validity of how much we can trust it. In a study by Johns and Yaffe<sup>[6]</sup> they used lead blocks method to measure SPR in a CT imaging system. In their study, they compared experimental and the simulation SPRs and observed a slight statistically negligible difference. Perhaps the most important and common method to evaluate and ensure a simulation results using experimental examination is to compare the intensity pattern of the pixels of simulated and simple experimental phantom images. However, in a study conducted by Thanasupsombat *et al.*,<sup>[29]</sup> a human-like head phantom was used. In addition, in a study by Najafi Darmian *et al.*,<sup>[36]</sup> GATE validation was done by comparing the scattering profile on a row detector of a CT scan between the simulation and the experimental exams. In our study, the quality control phantom of the chosen CT scan device was selected for testing and simulation. The results in three rows of the phantom were compared with each other in terms of pixel intensity pattern, and they were acceptable. Peak intensities in all areas were similar to each other. One of the upcoming challenges in CT scan simulation studies is the reconstruction of obtained projection images. We utilized OMEGA, a MATLAB-based program, to reconstruct images using the back projection method. As mentioned before, simulating cone-beam CTs with GATE is more common, and generally single-projection images are used in studies. One of the most important applications of GATE is to estimate the scatter of different imaging modalities to improve the final images by implementing scatter correction or rejection methods. In this study, we considered a scatter correction approach based on the Monte Carlo estimation method. In other studies, conducted based on this method, success rate has been highly dependent on a precise simulation and correct estimation based on the same simulation. However, the Monte Carlo technique has been highly effective due to its statistical and random nature.<sup>[29,37,38]</sup> In order to evaluate the success of GATE in scatter estimation more comprehensively, four quantities were investigated for scatter correction. The middle row, filled with water, has been chosen for pixel intensity evaluation in a uniform environment. In this uniform environment, it



is easier to evaluate the pattern and intensity of cupping artifacts caused by scattering. It is quite clear that cupping has decreased after scatter correction and the intensity of pixels (black color) has increased and improved. Reduction of the arc of the pixel intensity graph and getting closer to the midline are well-known signs of cupping decrease in CT scan images.

In CT number inaccuracy evaluation, after scatter correction the Teflon reached the lowest error about 1.89%. This difference has reached <10% in all absorption pins, which is desirable. CT scan number improvement after scatter correction is evident in all absorption pins in any considered case, according to the reference type. The most drastic improvement, shown in Table 3, belongs to CT number of water. All of these highlight the extent of scattered radiation's destructive effect on both the quality and the diagnostic accuracy of the CT scan images. In other words, they show how crucially important it is to reduce and remove scattered rays from images. All the calculated CNRs are below 50. The highest to lowest CNRs after scatter correction is respectively for Teflon, Lexan, polyethylene and acrylic. Before correction, of course, Teflon and Lexan had the highest CNRs. SNR intensity in the center of the phantom was the lowest SNR both before and after correction. Given that cupping effects generally involve the center of the phantoms, we can say that this low SNR in the center of the phantom was predictable and not far from expectation. Although a 67% of enhancement in SNR is observed after correction, this improvement is lower than that of other areas, especially for the top ROI with 150% signal-to-noise improvement. In fact, the top ROI has always had the highest SNR ratio. In a study conducted by Najafi Darmian *et al.*,<sup>[36]</sup> a 64-slice CT scan was simulated by the GATE program, and by checking the profile of the scatter rays and the SPR ratios, they validated this method and emphasized the effectiveness of the scatter estimation methods. Furthermore, in a study by Thanasupsombat *et al.*,<sup>[29]</sup> a cone-beam CT was simulated with a phantom similar to a human head, and the contrast ratio and intensity profile were compared in the images before and after scatter correction. In all images, after scatter correction, an increase in intensity profile and contrast has been observed. In another study by Thanasupsombat *et al.*,<sup>[37]</sup> the only feature of the inaccuracy of the CT number in the images after scatter correction has been investigated, which has again emphasized the effectiveness of scatter correction using Monte Carlo estimation method by GEANT4 in a CBCT. According to these studies and other studies, a CT scan with high-slice fan-beam geometry was selected in this study, and the most important factors involved in the quality of the images that can help in more correct diagnosis were investigated.

## Conclusion

The simulation of imaging systems such as CT by GATE programs based on Monte Carlo is known as a very

desirable method. In this study, we evaluated the accuracy of such simulation. Due to the random nature of both the physics of interactions in imaging systems and Monte Carlo-based processes, Monte Carlo-based programs are well able to simulate the processes of beam production and interactions. The proposed method for scatter correction of CT scan images includes estimating the scattering pattern by the GATE program and applying and using the same pattern to correct and remove the scattered rays. In conclusion, it should be said that the scatter correction of CT scan images using Monte Carlo-based GATE improved SNR, CNR, CT number accuracy, and image quality by enhancing pixel intensity. Therefore, it seems that by using the simulation of fan-beam CT scans and the estimation of scatter rays by Monte Carlo methods such as GATE, it is possible to scatter correction in CT scan images in clinical environments and increase the diagnostic.

## Acknowledgments

This research is supported by the School of Medicine, Iran University of Medical Sciences (IUMS) under Grant 20515.

## Financial support and sponsorship

None.

## Conflicts of interest

There are no conflicts of interest.

## References

1. Mazonakis M, Damilakis J. Computed tomography: What and how does it measure? *Eur J Radiol* 2016;85:1499-504.
2. Miwa K, Nemoto R, Masuko H, Yamao T, Kobayashi R, Miyaji N, *et al.* Evaluation of quantitative accuracy among different scatter corrections for quantitative bone SPECT/CT imaging. *PLoS One* 2022;17:e0269542.
3. Pauwels R, Pittayapat P, Sinpitaksakul P, Panmekiate S. Scatter-to-primary ratio in dentomaxillofacial cone-beam CT: Effect of field of view and beam energy. *Dentomaxillofac Radiol* 2021;50:20200597. doi: 10.1259/dmfr.20200597.
4. Glover GH. Compton scatter effects in CT reconstructions. *Med Phys* 1982;9:860-7.
5. Siewerdsen JH, Jaffray DA. Cone-beam computed tomography with a flat-panel imager: Magnitude and effects of X-ray scatter. *Med Phys* 2001;28:220-31.
6. Johns PC, Yaffe M. Scattered radiation in fan beam imaging systems. *Med Phys* 1982;9:231-9.
7. Joseph PM, Spital RD. The effects of scatter in X-ray computed tomography. *Med Phys* 1982;9:464-72.
8. Qu X, Lai CJ, Zhong Y, Yi Y, Shaw CC. A general method for cupping artifact correction of cone-beam breast computed tomography images. *Int J Comput Assist Radiol Surg* 2016;11:1233-46.
9. Pedote P, Cozzolino M, Nicolardi M, Accogli RU, Sardaro A, Scardapane A, *et al.* Streak artefacts in computed tomography urography: Comparative evaluation between two different iodinated contrast media. *J Med Imaging Radiat Oncol* 2022;66:940-5.
10. Jarry G, Graham SA, Moseley DJ, Jaffray DJ, Siewerdsen JH,

- Verhaegen F. Characterization of scattered radiation in kV CBCT images using Monte Carlo simulations. *Med Phys* 2006;33:4320-9.
11. Kyriakou Y, Riedel T, Kalender WA. Combining deterministic and Monte Carlo calculations for fast estimation of scatter intensities in CT. *Phys Med Biol* 2006;51:4567-86.
  12. Rührschopf EP, Klingenberg K. A general framework and review of scatter correction methods in X-ray cone-beam computerized tomography. Part 1: Scatter compensation approaches. *Med Phys* 2011;38:4296-311.
  13. Rührschopf And EP, Klingenberg K. A general framework and review of scatter correction methods in cone beam CT. Part 2: Scatter estimation approaches. *Med Phys* 2011;38:5186-99.
  14. Boone JM, Seibert JA. An analytical model of the scattered radiation distribution in diagnostic radiology. *Med Phys* 1988;15:721-5.
  15. Kanamori H, Nakamori N, Inoue K, Takenaka E. Effects of scattered X-rays on CT images. *Phys Med Biol* 1985;30:239-49.
  16. Honda M, Kikuchi K, Komatsu K. Method for estimating the intensity of scattered radiation using a scatter generation model. *Med Phys* 1991;18:219-26.
  17. Kalender W. Monte Carlo calculations of X-ray scatter data for diagnostic radiology. *Phys Med Biol* 1981;26:835-49.
  18. Chan HP, Doi K. Physical characteristics of scattered radiation in diagnostic radiology: Monte Carlo simulation studies. *Med Phys* 1985;12:152-65.
  19. Zaidi H, Ay MR. Current status and new horizons in Monte Carlo simulation of X-ray CT scanners. *Med Biol Eng Comput* 2007;45:809-17.
  20. Agostinelli S, Allison J, Amako K, Apostolakis J, Araujo H, Arce P, *et al.* Geant4 – A simulation toolkit. *Nucl Instrum Methods Phys Res Sect A* 2003;506:250-303. [doi: 10.1016/S0168-9002(03)01368-8].
  21. Jan S, Santin G, Strul D, Staelens S, Assié K, Autret D, *et al.* GATE – Geant4 application for tomographic emission: A simulation toolkit for PET and SPECT. *Phys Med Biol* 2004;49:4543-61.
  22. Punnoose J, Xu J, Sisniega A, Zbijewski W, Siewerdsen JH. Technical note: SPEKTR 3.0-A computational tool for X-ray spectrum modeling and analysis. *Med Phys* 2016;43:4711.
  23. Jan S, Santin G, Strul D, Staelens S, Assié K, Autret D, *et al.* GATE: A simulation toolkit for PET and SPECT. *Phys Med Biol* 2004;49:4543-61.
  24. Asai M, Cortés-Giraldo MA, Giménez-Alventosa V, Giménez Gómez V, Salvat F. The PENELOPE physics models and transport mechanics. Implementation into Geant4. *Front Phys* 2021;9. doi: 10.3389/fphy.2021.738735
  25. Brun R, Rademakers F. ROOT – An object oriented data analysis framework. *Nucl Instrum Methods Phys Res Sect A* 1997;389:81-6.
  26. Wettenhovi VV, Vauhkonen M, Kolehmainen V. OMEGA-open-source emission tomography software. *Phys Med Biol* 2021;66:065010.
  27. Schneider CA, Rasband WS, Eliceiri KW. NIH image to ImageJ: 25 years of image analysis. *Nat Methods* 2012;9:671-5.
  28. Gao H, Fahrig R, Bennett NR, Sun M, Star-Lack J, Zhu L. Scatter correction method for X-ray CT using primary modulation: Phantom studies. *Med Phys* 2010;37:934-46.
  29. Thanasupsombat C, Thongvigitmanee SS, Aootaphao S, Thajchayapong P. A simple scatter reduction method in cone-beam computed tomography for dental and maxillofacial applications based on Monte Carlo simulation. *Biomed Res Int* 2018;2018:5748281.
  30. Ay MR, Zaidi H. Development and validation of MCNP4C-based Monte Carlo simulator for fan- and cone-beam X-ray CT. *Phys Med Biol* 2005;50:4863-85.
  31. Colijn AP, Beekman FJ. Accelerated simulation of cone beam X-ray scatter projections. *IEEE Trans Med Imaging* 2004;23:584-90.
  32. Malusek A, Sandborg M, Carlsson GA. CTmod-a toolkit for Monte Carlo simulation of projections including scatter in computed tomography. *Comput Methods Programs Biomed* 2008;90:167-78.
  33. Zbijewski W, Beekman FJ. Efficient Monte Carlo based scatter artifact reduction in cone-beam micro-CT. *IEEE Trans Med Imaging* 2006;25:817-27.
  34. Mainegra-Hing E, Kawrakow I. Fast monte carlo calculation of scatter corrections for CBCT images. *J Phys Conf Ser* 2008;102:012017.
  35. Mainegra-Hing E, Kawrakow I. Variance reduction techniques for fast Monte Carlo CBCT Scatter correction calculations. *Phys Med Biol* 2010;55:4495-507.
  36. Najafi Darmian A, Ay MR, Pouladian M, Shirazi A, Ghadiri H, Akbarzadeh A, *et al.* Characterization of scattered radiation profile in volumetric 64 slice CT scanner: Monte carlo study using GATE. In: *IEEE nuclear science symposium conference record*; 2011. p. 2692-6.
  37. Thanasupsombat C, Pengvanich P, Aootaphao S, Thongvigitmanee SS. A Post-Processing Method for Improving Contrast and Reducing Cupping Artifacts in Low-Energy CBCT Images; 2013. p. 4-6.
  38. Baer M, Hammer M, Knaup M, Schmidt I, Christoph R, Kachelrieß M. Scatter correction methods in dimensional CT. 4th conference on industrial computed tomography (iCT). Wels, Austria: e-Journal Nondestr Test 2012;17.